

# CVD Growth Control and Separation of Single-Walled Carbon Nanotubes for FET Devices

Shigeo Maruyama<sup>1</sup>

<sup>1</sup>Department of Mechanical Engineering, The University of Tokyo  
7-3-1 Hongo, Bunkyo-ku, Tokyo 113-8656, Japan

## §1 Introduction

Chemical vapor deposition (CVD) growth control and density gradient ultracentrifugation (DGU) separation were developed for the practical use of single-walled carbon nanotubes (SWNTs) in electronic and optical devices. Based on the explored CVD growth mechanism of alcohol catalytic CVD (ACCVD), diameter controlled growth of vertically aligned SWNTs (VA-SWNTs), growth of nitrogen-doped SWNT, patterned growth of VA-SWNTs, horizontally aligned growth are realized. DGU separation of each chirality of SWNTs and of semiconductor and metallic SWNTs are also demonstrated. Raman and photoluminescence (PL) spectroscopy are developed using the single-chirality dispersion sample. Finally, several field effect transistors (FET) are demonstrated using as-grown SWNTs.

## §2 Chemical reaction in CVD process and diameter control

The gas-phase decomposition of carbon source molecule (ethanol for ACCVD) before the reaction with metal catalysts is revealed to be very important [1-3]. As shown in Fig. 1[4], ethanol decomposition determine the strong flow-rate dependent growth curves of VA-SWNTs observed by *in situ* laser absorption [5,6]. Especially, tiny amount of decomposed acetylene highly accelerates the SWNT growth but at the same time promotes the deactivation of small catalyst by carbon over-coating [7]. The highly efficient polymerization reaction of acetylene can be observed from direct reaction experiment of size-selected metal clusters with Fourier transform ion cyclotron resonance (FT-ICR) mass-spectrometer [8].

No-flow ACCVD maximizing the decomposition [9] was developed for efficient growth of VA-SWNTs even from ethanol with <sup>13</sup>C isotope [10]. The root-growth model (metal catalysts is staying in substrate) was confirmed with such isotope experiments [10]. Hence, carbon source molecules need to diffuse through

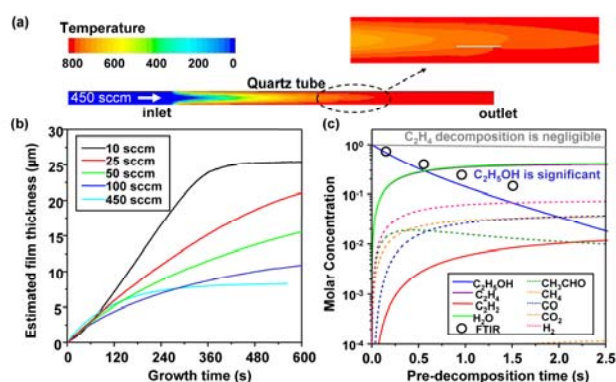


Figure 1. (a) Temperature distribution inside the quartz tube during CVD. (b) Growth curves of SWNTs at 800 °C for different ethanol flow rates. (c) Ethanol decomposition process calculated by the chemical dynamics simulation, and measured ethanol concentrations (circles) by FTIR.

SWNT array before the catalytic reaction near the substrate. The diffusion barrier was estimated to be small for VA-SWNTs with thickness less than 1 mm [11]. Furthermore, effect of metal particles and effect of catalyst support are studied employing combinatory experiments [12] and surface plane defined silicate [13], respectively. Based on these findings, the nanotube diameter of VA-SWNTs was controlled by CVD process parameters [14].

Recently, a strikingly small diameter (around 0.7 nm) VA-SWNTs was achieved by mixing acetonitrile to ethanol feedstock as shown in Fig. 2 [15]. With increasing acetonitrile concentration in the feedstock, nitrogen incorporation into the  $sp^2$  carbon network increased until saturating at approximately one atomic percent. The incorporation of nitrogen correlates with a significant diameter reduction from a mean diameter of 2.1 nm down to 0.7 nm.

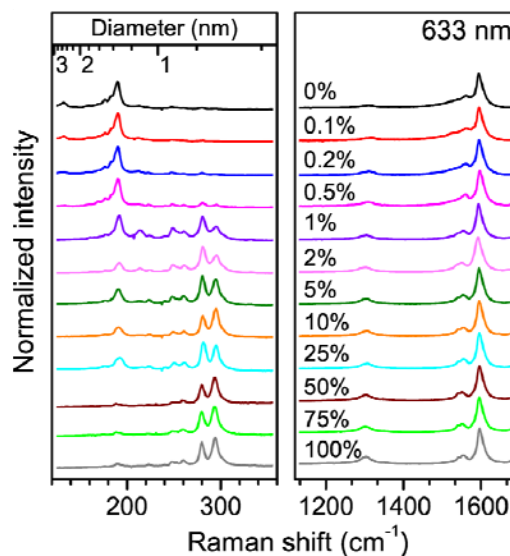


Figure 2. Resonance Raman spectra at 633 nm excitation of VA-SWCNT arrays grown using ethanol-acetonitrile mixture, with different acetonitrile concentrations.

### §3 DGU Separation of chirality and metal/semiconductor

Since the single-chirality SWNT growth is still challenging, development of separation technique is inevitable. We present a protocol to selectively isolate SWNTs with different chiralities in a full-colored “rainbow” expansion using DGU [16]. Starting with SWNTs synthesized by ACCVD method, we used sodium deoxycholate (DOC) and sodium dodecyl sulfate (SDS) as cosurfactant encapsulating agents to form a DOC-restricted SDS wrapping morphology around the SWNTs. This enhances the density differences between nanotubes of different diameters, which leads to efficient chirality redistribution when combined with an appropriate density gradient profile as shown in Fig. 3 [16].

Through a systematic study of the effects of surfactants, analysis of the buoyant densities, layer positions, and optical absorbance spectra of SWNT separations using DOC and SDS, we clarify the roles and interactions of these two surfactants in yielding different DGU outcomes [17]. The separation mechanism described in Ref. [17] can also help in designing new DGU experiments by qualitatively predicting outcomes of different starting recipes,

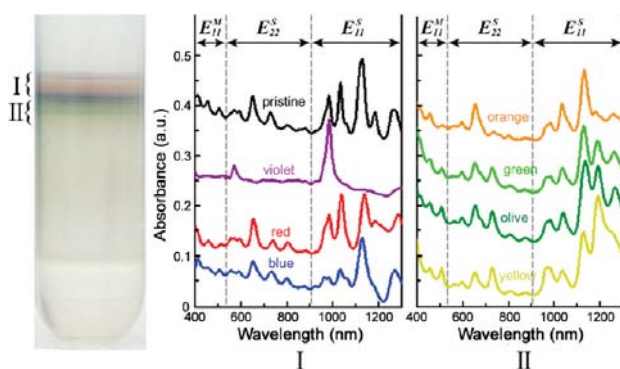


Figure 3. Left: Photograph showing multilayered separation “rainbow” of ACCVD SWNTs by DGU. Right: Optical absorbance spectra of each colored fraction.

improving the efficacy of DGU and simplifying post-DGU fractionation.

#### §4 Development of optical spectroscopy of SWNTs

Raman and PL spectroscopy are further developed through theoretical studies and experimental studies. Radial breathing mode (RBM) intensity was calculated through exciton-photon and exciton-phonon interaction matrix elements within extended tight binding method [18]. Resonance Raman intensity for RBM as a function of diameter and chiral angle are summarized, which should be combined with Kataura plot for chirality assignment of Raman peaks.

Polarization dependence of RBM mode peaks of VA-SWNTs revealed that the anomalous RBM peaks previously attributed to perpendicularly polarized excitation is actually from parallel polarized excitation of isolated SWNTs suspended within the array [19]. Isotope-induced elastic scattering of optical phonons in individual suspended SWNTs are studied [20].

Several important spectroscopic features in PL signal were found. We performed detailed PL spectroscopy studies of three different types of SWNTs by using samples that contain essentially only one chiral type of SWNT, (6,5), (7,5), or (10,5). The observed PL spectra unambiguously show the existence of an emission sideband at about 140 meV below the lowest singlet excitonic  $E_{11}$  level. We ascribe the origin of the observed sideband to coupling between K-point phonons and dipole-forbidden dark excitons [21].

The asymmetry between valence and conduction bands in SWNTs was studied through the direct observation of spin-singlet transverse dark excitons using polarized PL excitation spectroscopy [22]. As shown in Fig. 4, the intrinsic electron-hole asymmetry lifts the degeneracy of the transverse exciton wave functions at two equivalent K and K' valleys, which gives finite oscillator strength to transverse dark exciton states.

#### §5 Position and alignment controlled CVD growth

The patterned growth of SWNTs were developed by patterning of  $\text{SiO}_2$  layer [23] and by patterning self-assembled monolayer (SAM) film [24]. The first approach [23] is the conventional concept of using  $\text{SiO}_2$  patterned Si substrates to selectively grow 3D carbon nanotube structures. High-quality VA-SWNT

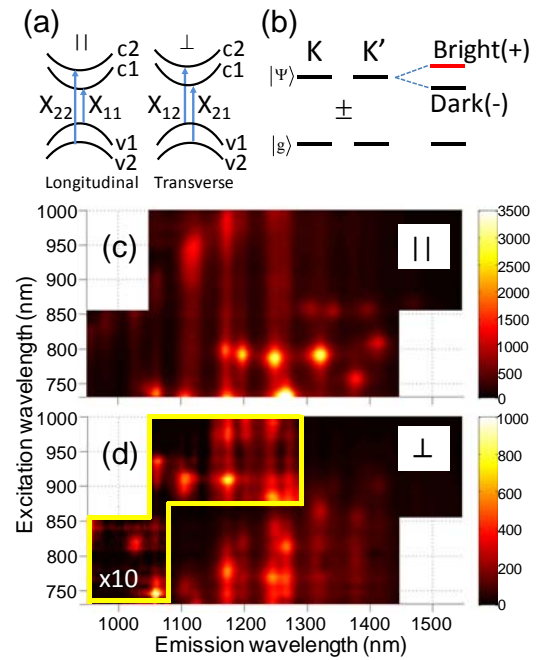


Figure 4. Schematic diagram of (a) the selection rules for incident light polarized parallel ( $\parallel$ ) and perpendicular ( $\perp$ ) to the nanotube axis, and (b) intervalley mixing of K and K' excitons. The superposition of wavefunctions near the K and K' points gives the bright and dark states for longitudinal and transverse excitons. PLE maps for excitations polarized (c) parallel ( $\parallel$ ) and (d) perpendicular ( $\perp$ ) to the nanotube axis.

patterns can be easily obtained by this protocol. Apart from the sintering of catalyst into Si at high temperature, the difference in surface wettability between Si and SiO<sub>2</sub> also plays an important role in this selective growth, which leads us to a novel method of patterning the growth on chemically modified surfaces. The latter approach [24] shown in Fig. 5 is based on the substrate wettability, which is found to be critical for the yield of SWNTs. On an OH-terminated hydrophilic Si/SiO<sub>2</sub> surface, the growth can be promoted by 10 times, but can be completely suppressed on a CH<sub>3</sub>-terminated hydrophobic surface. Selective surface modification is utilized to localize the growth of SWNTs. The proposed technique has advantages in improved simplicity and potentially better resolution compared to conventional lithography.

We used both R-cut and R-face crystal quartz substrates for the efficient growth of horizontally aligned SWNTs [25]. The R-plane (10-11) is one of the low-index crystallographic planes of crystal quartz. The surface cut from a synthetic quartz block parallel to the R-plane was used as R-cut substrates, and the exposed R-plane was used as R-face substrates. We elucidated that the atomic structure of the R-plane causes the alignment of the SWNTs. While a step-and-terrace structure clearly appeared on R-face substrates, SWNTs were aligned on the terraced area of the R-plane, regardless of the direction of the step edges. Comparison between R-face and ST-cut substrates suggests that the ST-cut surface can be considered as a collection of tiny r-plane (01-11) domains, which are very similar to the R-plane (10-11).

We found the density of horizontally aligned SWNTs depends on partial pressures of carbon source gas [26]. We also examined the time devolution of horizontally aligned SWNT. By extending and broadening the distribution of the incubation time, high-density horizontally aligned SWNTs were achieved as shown in Fig. 6.

## §6 All-carbon flexible FET

A carbon nanotube FET is a promising candidate for future electronic devices; however, its fabrication process is still challenging.

We propose a simple fabrication technique for CNT-FET arrays using as-grown SWNTs as the gate channel

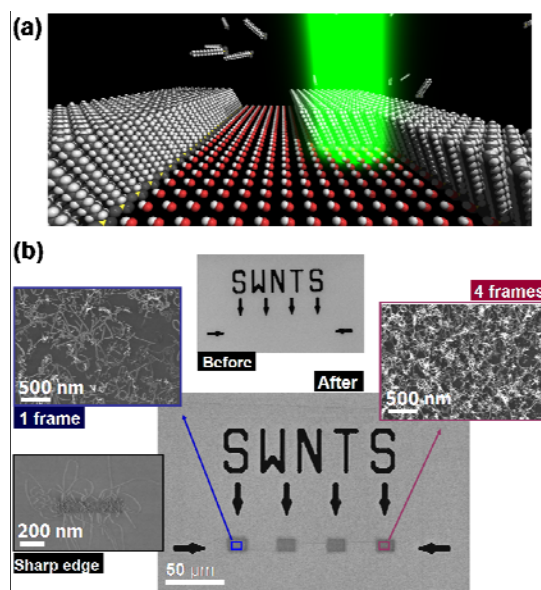


Figure 5 (a) Schematics describing the process of removing OTS SAM by nanometer-size electron beam; (b) SEM images of SWNTs grown in the regions where OTS were selectively removed, suggesting the location and density of SWNTs can be controlled.

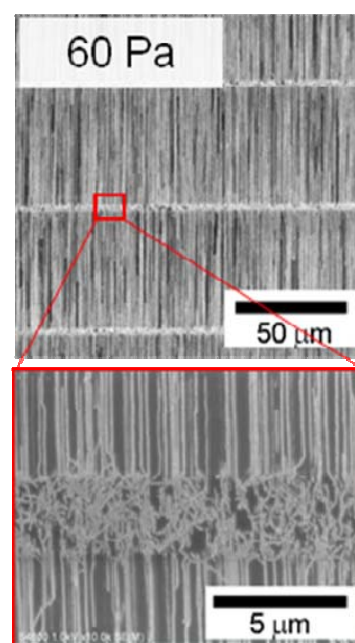


Figure 6. Density controlled CVD growth of horizontally aligned SWNTs on R-cut crystal quartz substrate.

[27].

Later, we have demonstrated CNT-FET using as-grown SWNTs for the channel as well as both source and drain electrodes. The underlying Si substrate was employed as the back-gate electrode. As shown in Fig. 7, patterned VA-SWNTs was used for electrodes [28]. The electrodes and channel were grown simultaneously in one CVD process. The resulting FETs exhibited  $I_{ON}/I_{OFF}$  ratios exceeding  $10^6$  and a maximum ON-state current of more than  $13 \mu\text{A}$ .

Finally, we demonstrated polymer-laminated, transparent, all-carbon-nanotube FET, making use of the flexible yet robust nature of SWNTs as shown in Fig. 8. All components of the FET (active channel, electrodes, dielectric layer, and substrate) consist of carbon-based materials. The use of a plastic substrate that is considerably thinner than those used in other flexible CNT-FETs allowed our devices to be highly deformable without degradation of electrical properties [29].

### Acknowledgement

Part of this work was financially supported by Grant-in-Aid for Scientific Research (19054003 and 22226006), JSPS Core-to-Core Program, and Global COE Program 'Global Center for Excellence for Mechanical Systems Innovation'.

### References

1. H. Sugime, S. Noda, S. Maruyama and Y. Yamaguchi, *Carbon* **47**, 234 (2009).
2. B. Hou, R. Xiang, T. Inoue, E. Einarsson, S. Chiashi, J. Shiomi, A. Miyoshi and S. Maruyama, *Jpn. J. App. Phys.* **50**, 065101 (2011).
3. H. Sugime and S. Noda, *Carbon* **50**, 2953 (2012).
4. R. Xiang, E. Einarsson, J. Shiomi and S. Maruyama, *J. Heat Transf.-Trans. ASME* **134**, 051023 (2012).
5. E. Einarsson, Y. Murakami, M. Kadowaki and S. Maruyama, *Carbon* **46**, 923 (2008).
6. E. Einarsson, M. Kadowaki, K. Ogura, J. Okawa, R. Xiang, Z. Zhang, T. Yamamoto, Y. Ikuhara and S. Maruyama, *J. Nanosci. Nanotech.* **8**, 6093 (2008).

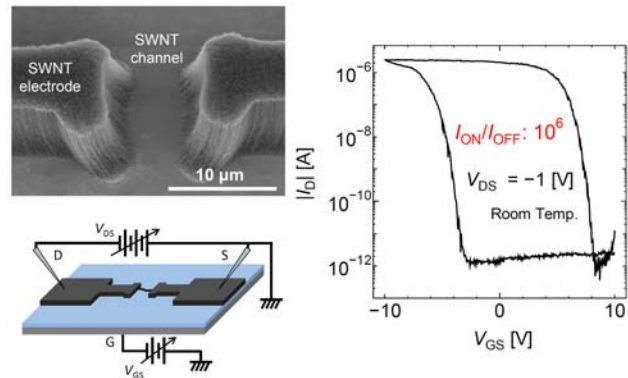


Figure 7. Fabricated FET using as-grown SWNTs for the channel as well as both electrodes.

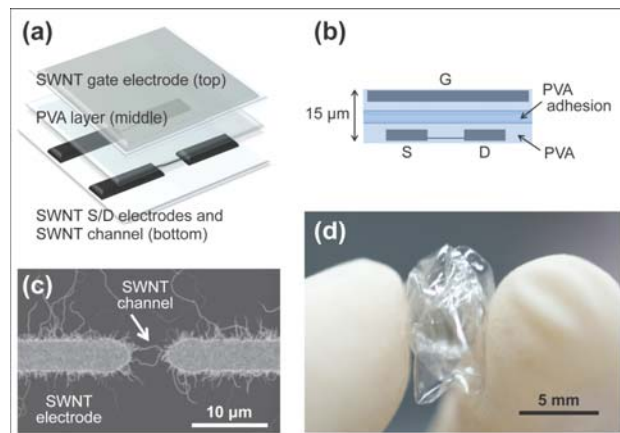


Figure 8. (a) Schematic of the layered structure of fabricated transparent all-CNT-FETs. (b) Schematic cross-section diagram of the device. (c) SEM image of the FET channel region obtained prior to removal from the master Si substrate. (d) Photograph of a crumpled, yet functional, all-CNT-FET device.

7. R. Xiang, E. Einarsson, J. Okawa, Y. Miyauchi and S. Maruyama, *J. Phys. Chem. C* **113**, 7511 (2009).
8. S. Inoue and S. Maruyama, *Jpn. J. Appl. Phys.* **47**, 1931 (2008).
9. H. Oshima, Y. Suzuki, T. Shimazu and S. Maruyama, *Jpn. J. Appl. Phys.* **47**, 1982 (2008).
10. R. Xiang, Z. Zhang, K. Ogura, J. Okawa, E. Einarsson, Y. Miyauchi, J. Shiomi and S. Maruyama, *Jpn. J. Appl. Phys.* **47**, 1971 (2008).
11. R. Xiang, Z. Yang, Q. Zhang, G. Luo, W. Qian, F. Wei, M. Kadowaki, E. Einarsson and S. Maruyama, *J. Phys. Chem. C* **112**, 4892 (2008).
12. H. Sugime and S. Noda, *Carbon* **48**, 2203 (2010).
13. T. Moteki, Y. Murakami, S. Noda, S. Maruyama and T. Okubo, *J. Phys. Chem. C* **115**, 24231 (2011).
14. T. Thurakitsee, E. Einarsson, R. Xiang, P. Zhao, S. Aikawa, S. Chiashi, J. Shiomi and S. Maruyama, *J. Nanosci. Nanotech.* **12**, 370 (2012).
15. T. Thurakitsee, C. Kramberger, P. Zhao, S. Aikawa, S. Harish, S. Chiashi, E. Einarsson and S. Maruyama, *Carbon* **50**, 2635 (2012).
16. P. Zhao, E. Einarsson, R. Xiang, Y. Murakami and S. Maruyama, *J. Phys. Chem. C* **114**, 4831 (2010).
17. P. Zhao, E. Einarsson, G. Lagoudas, J. Shiomi, S. Chiashi and S. Maruyama, *Nano Res.* **4**, 623 (2011).
18. K. Sato, R. Saito, A.-R. T. Nugraha and S. Maruyama, *Chem. Phys. Lett.* **497**, 94 (2010).
19. Z. Zhang, E. Einarsson, Y. Murakami, Y. Miyauchi and S. Maruyama, *Phys. Rev. B* **81**, 165442 (2010).
20. P. Zhao, E. Einarsson, R. Xiang, Y. Murakami, S. Chiashi, J. Shiomi and S. Maruyama, *Appl. Phys. Lett.* **99**, 093104 (2011).
21. Y. Murakami, B. Lu, S. Kazaoui, N. Minami, T. Okubo and S. Maruyama, *Phys. Rev. B* **79**, 195407 (2009).
22. Y. Miyauchi, H. Ajiki and S. Maruyama, *Phys. Rev. B* **81**, 121415 (2010).
23. R. Xiang, E. Einarsson, H. Okabe, S. Chiashi, J. Shiomi and S. Maruyama, *Jpn. J. Appl. Phys.* **49**, 02BA03 (2010).
24. R. Xiang, T. Wu, E. Einarsson, Y. Suzuki, Y. Murakami, J. Shiomi and S. Maruyama, *J. Am. Chem. Soc.* **131**, 10344 (2009).
25. S. Chiashi, H. Okabe, T. Inoue, J. Shiomi, T. Sato, S. Kono, M. Terasawa and S. Maruyama, *J. Phys. Chem. C* **116**, 6805 (2012).
26. T. Inoue, D. Hasegawa, S. Badar, S. Chiashi and S. Maruyama, to be submitted.
27. S. Aikawa, E. Einarsson, T. Inoue, R. Xiang, S. Chiashi, J. Shiomi, E. Nishikawa and S. Maruyama, *Jpn. J. Appl. Phys.* **50**, 04DN08 (2011).
28. S. Aikawa, R. Xiang, E. Einarsson, S. Chiashi, J. Shiomi, E. Nishikawa and S. Maruyama, *Nano Res.* **4**, 580 (2011).
29. S. Aikawa, E. Einarsson, T. Thurakitsee, S. Chiashi, E. Nishikawa and S. Maruyama, *Appl. Phys. Lett.* **100**, 063502 (2012).

**Corresponding Author: S. Maruyama**

**Email: maruyama@photon.t.u-tokyo.ac.jp**